Acta Crystallographica Section B
Structural Science
ISSN 0108-7681

Experimental and theoretical charge-density study of a tetranuclear cobalt carbonyl complex

Jacob Overgaard,[a]* Jamie A. Platts[b] and Bo B. Iversen[b]

[a]Department of Chemistry, Aarhus University, Denmark, and [b]School of Chemistry, University of Cardiff, Wales

Correspondence e-mail: jacobo@chem.au.dk

Received 18 August 2009
Accepted 28 October 2009

Details of the complex bonding environment present in the molecular centre of an alkyne-bridged dicobalt complex have been examined using a combination of experimental and theoretical charge-density modelling for two compounds which share a central Co_2C_2 tetrahedral moiety as their common motif. Topological analysis of the experimental electron density illustrates the problem of separating the Co—C bond-critical points (b.c.p.s) from the intervening ring-critical point (r.c.p.), due largely to the flat nature of the electron density in the CoC_2 triangles. Such a separation of critical points is immediately obtained from a topological analysis of the theoretical electron density as well as from the multipole-projected theoretical density; however, the addition of random noise to the theoretical structure factors prior to multipole modelling leads to a failure in consistently distinguishing two b.c.p.s and one r.c.p. in such close proximity within the particular environment of this Co_2C_2 centre.

1. Introduction

There is an ongoing discussion in the literature on the nature of the chemical bonding between transition metals in bridged dimers of the type $M_2(CO)_xR$, where x varies with the metal atom type and R is a bridging ligand, which may be another carbonyl group. Pioneering experimental charge-density studies by Macchi on a series of coordination complexes showed that direct metal–metal bonding disappears as the two atoms become bridged by a carbonyl group (Macchi *et al.*, 1999). Farrugia and co-workers (Farrugia *et al.*, 2003; Farrugia & Evans, 2005) as well as other groups (Macchi, 2005; Flierler *et al.*, 2008; Bianchi *et al.*, 1998, 2001; Overgaard *et al.*, 2008) have also studied the charge density in metal–metal bonded complexes using the experimental charge-density approach. The common method in these studies is the implementation of a topological analysis of the whole electron density based on the quantum theory of atoms in molecules (QTAIM) developed by Bader (1990). The issue has been theoretically studied by Gatti using the source function (Bader & Gatti, 1998; Gatti & Lasi, 2007) which is able to distinguish between bonding or non-bonding in metal dimers. An alternative to the conventional QTAIM analysis is the use of the kinetic and potential energy density, originally proposed by Cremer & Kraka (1984*a*,*b*) and recently used by Finger & Reinhold (2003) in this context. In this paper we describe the experimental electron-density distribution in an alkyne-bridged carbonyl complex, $Co_4(CO)_{12}PhC{\equiv}C{-}C{\equiv}CPh$ (1), determined from multipole modelling of single-crystal X-ray diffraction data collected at liquid N_2 temperatures. The experimental results are combined with the results of gas-phase theoretical calcu-

Table 1
Crystallographic details and refinement statistics for (1).

Crystal data	
Chemical formula	$C_{28}H_{10}Co_4O_{12}$
M_r	774.08
Crystal system	Monoclinic, $P2_1/n$
Temperature (K)	90
a, b, c (Å)	8.8195 (3), 17.5085 (5), 18.3080 (5)
β (°)	90.4440 (10)
V (Å^3)	2826.97 (15)
$F(000)$	1528
D_x (Mg m^3)	1.819
Radiation type	Mo $K\alpha$
μ (mm^{-1})	2.37
Crystal size	0.55 × 0.24 × 0.15
Data collection	
Diffractometer	Bruker X8 APEXII
Absorption correction	Gaussian
T_{min}, T_{max}	0.288, 0.737
d_{min} (Å)	0.42
No. of measured, independent and observed [$I > 2\sigma(I)$] reflections	252 043, 33 537, 27 825
Average redundancy	7.5
Completeness (%)	86.4
No. of discarded reflections	53
R_{int}	0.0234
Range of h, k, l	$h = -20 \rightarrow 20, k = 0 \rightarrow 40, l = 0 \rightarrow 40$
Multipole refinement	
$R[F^2 > 2\sigma(F)]$, $wR(F^2)$, S	0.016, 0.021, 1.53
No. of reflections	27 825
No. of parameters	677
No. of restraints	0
Weighting scheme	$w^2 = 1/[\sigma^2(F_o^2)]$
$\Delta\rho_{max}$, $\Delta\rho_{min}$ (e Å^{-3})	0.52, −0.58

Computer programs used: *APEX*2 (Bruker, 2007*a*), *SAINT*+ (Bruker, 2007*b*), *XD*2006 (Volkov *et al.*, 2006).

lations of (1). In a previous study of a related complex (Overgaard *et al.*, 2008), $Co_2(CO)_6(HC{\equiv}CC_6H_{10}OH)$, we showed that a direct Co—Co bond is not present, and that experimental determination of the electron density has difficulty in identifying all the expected Co—C bonds. Theoretical calculations also indicated significant singlet biradical character in (1), thus requiring multi-reference complete active-space self-consistent field (CASSCF) calculations to properly describe the electronic structure of such compounds. The quality of the data obtained in this work, coupled with the rather simpler crystalline environment observed for (1) (Z' is 2 for the related, previously studied complex), allows us to probe in more detail these effects and any shortcomings in describing them stemming from standard treatments of experimental electron-density analysis.

Owing to the large size of complex (1), theoretical structure factors were instead derived for a similar but smaller complex approximately half the size of (1) ($[Co(CO)_3]_2PhC{\equiv}CPhNO_2$ (2), Fig. 1*b*). Recently, we determined the electron-density distribution in this compound based on experimental single-crystal X-ray diffraction data that apparently lacked the quality that would justify their publication. However, the findings in the study prompted us to search for a suitable replacement that is presented here as (1). Theoretical structure factors calculated for (2) form the basis for multipole modelling, such that comparison of direct and multipole-modelled theoretical electron-density properties allow us to better understand the performance of this approach for such complexes. Subsequently, experimental noise was added to this set of theoretically generated structure factors in order to establish the influence that this may have on the finer details of the density distribution within the Co_2C_2 environment.

2. Experimental

2.1. Data collection and refinement of (1)

Complex (1) was prepared according to literature directives (Greenfield *et al.*, 1956). A black single crystal of size 0.13 × 0.21 × 0.53 mm was used for data collection on a Bruker Kappa Apex2 diffractometer at Aarhus University. The crystal was cooled to 90 (1) K using an Oxford Cryosystems N_2 cooling device. Complete coverage in reciprocal space was obtained in four days using a combination of φ and ω

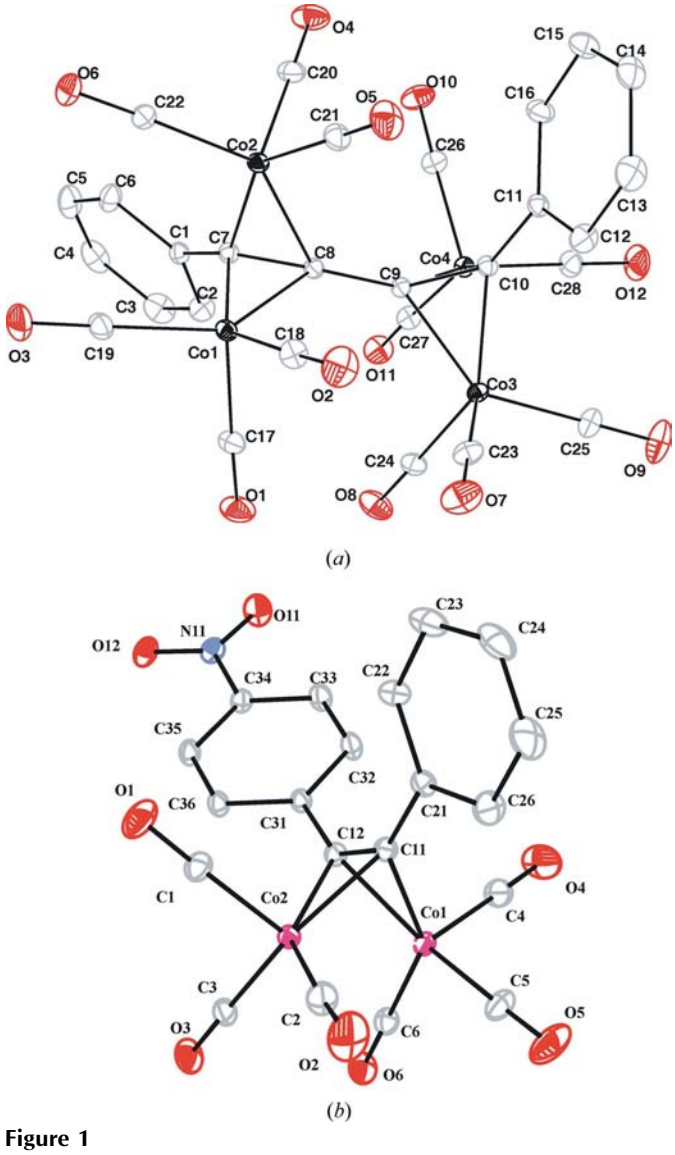

Figure 1
ORTEP view of (*a*) (1) and (*b*) (2). The ellipsoids show 90% probability surfaces. The H atoms have been omitted for clarity.

scans of 0.5°. The data was integrated using *SAINT*+ (Bruker, 2007*b*) to give 252 043 reflections, which were corrected for absorption using the Gaussian face-indexed procedure available in *SADABS* (Sheldrick, 2008). Equivalent reflections were merged in *SORTAV* (Blessing, 1989, 1997), which led to 33 537 unique reflections. The structure was solved by direct methods (*SHELXS*97) and an independent atom model (IAM) was refined to convergence using *SHELXL*97 (Sheldrick, 2008). The H atoms could all be located in a difference-Fourier analysis but they were initially positioned in calculated positions. The residuals from the IAM refinement were: $R(F)$ = 0.035 and $wR(F^2)$ = 0.061 for all data, and the difference-Fourier function showed peaks in the bonding regions. The experimental details are given in Table 1.

To model the electron-density distribution in (1), the above IAM model was imported into the multipole refinement program package *XD*2006 (Volkov *et al.*, 2006), which uses the Hansen–Coppens electron-density description (Hansen & Coppens, 1978). The first step in this procedure was to make a refinement using F^2 of the positional and displacement parameters against the high-order data [$\sin\theta/\lambda > 0.9$ Å^{-1}; 12 071 reflection with $I > 2\sigma(I)$]. This set of atomic parameters, which gives an average value of the difference of mean-square displacement amplitudes of 3.0×10^{-4} Å^2 (excluding bonds between atoms of dissimilar masses) and thus clearly fulfilling the Hirshfeld rigid-bond test (Hirshfeld, 1976), was kept fixed in the following refinements. The H atoms were from this point on displaced along their bond vectors to give bond distances corresponding to tabulated and averaged values compiled from neutron experiments (Allen *et al.*, 1987). The isotropic displacement parameters that resulted from the IAM refinements were simply retained until anisotropic parameters were derived (see later). The multipole parameters were now introduced to give a final model with maximum multipole levels of 4 on Co, 3 on O and C, while for all H atoms a monopole and bond-directed dipole and quadrupole was shared. For atoms in the phenyl rings, a non-crystallographic mirror plane was maintained to constrain a selection of parameters to a value of zero. The radial parameters, κ and κ', were divided into six sets, one for each atom type except C, for which three types (aromatic, alkyne and carbonyl) were used. Using this structural model a rigid-body (TLS) analysis (Schomaker & Trueblood, 1968) was performed with each of the phenyl rings comprising an attached rigid group. Then, combining the refined TLS parameters from this approach with calculated internal vibrational amplitudes for similar H-atom types as incorporated in the online program *SHADE*2 (Madsen, 2006; Munshi *et al.*, 2008), anisotropic atomic displacement parameters were derived for the H atoms and included in the model. Then, two final refinements were carried out, the first adjusting the atomic and displacement parameters and the final one the multipole parameters alone. The final model with 676 parameters refined with 27 825 reflections [$I > 2\sigma(I)$] leads to $R(F^2)$ = 0.017 and $wR(F^2)$ = 0.022. The fractal distribution of the residual density is rather parabolic in shape as shown in Fig. 2 with $d^f(0)$ = 2.80, which is actually a higher value than any of the examples presented in the original paper describing this procedure (Meindl & Henn, 2008), suggesting a successful refinement. The residual unsurprisingly reaches a maximum near the Co atoms as seen in the residual density map (Fig. 3).

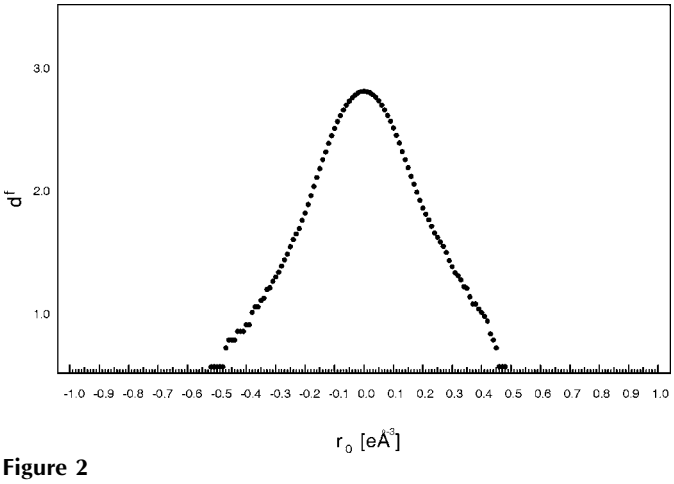

Figure 2
Fractal distribution of the residual density of (1). The calculation includes all data.

2.2. Theoretical calculations

Compound (1) is too large to treat at the CASSCF level, so instead density-functional theory (DFT) was employed to generate the electron density. In previous studies we showed that the BLYP functional (Becke, 1988; Lee *et al.*, 1988) reproduced most of the important features of the CASSCF

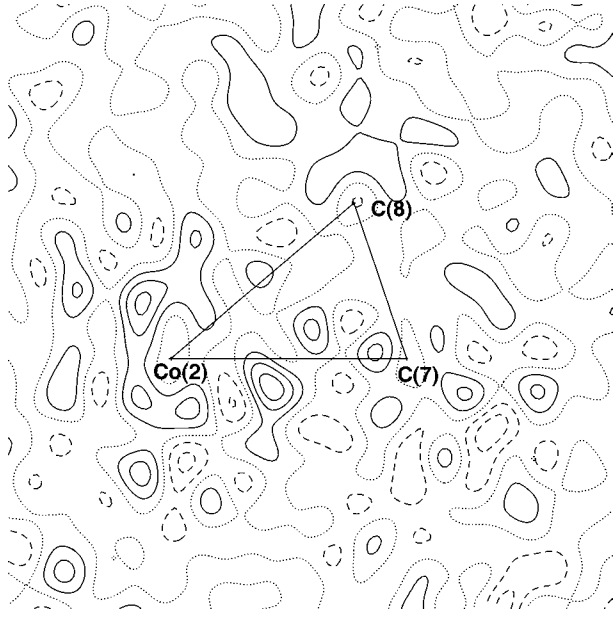

Figure 3
Residual density map in the plane spanned by the three atoms: Co2, C7 and C8. The contour interval is 0.10 e Å^{-3}, solid lines for positive contours and dashed lines for negative. Other sections of the unit cell are shown in the supplementary material.

Table 2
Geometrical and topological properties at the b.c.p.s in (1).

The first line gives the experimental values and the second line gives the theoretical results.

Bond	d (Å)	$\rho(\mathbf{r}_c)$ (e Å^{-3})	$\nabla^2\rho(\mathbf{r}_c)$ (e Å^{-5})	R_{12} (Å)	$d_{1\text{-b.c.p.}}$ (Å)	λ_1 (e Å^{-5})	λ_2 (e Å^{-5})	λ_3 (e Å^{-5})	ε
Co1—C7	1.9832 (2)	0.62 (1)	7.96 (1)	1.998	1.017	−2.60	−0.69	11.25	2.77
		0.667	7.075		1.013	−2.82	−1.67	11.57	0.68
Co1—C8	1.9735 (2)	0.63 (1)	8.28 (1)	1.990	1.013	−2.53	−0.85	11.66	1.97
		0.676	7.215		1.007	−2.90	−1.82	11.94	0.59
Co1—C17	1.8011 (3)	0.92 (1)	12.51 (1)	1.801	0.923	−4.68	−4.64	21.83	0.01
		0.943	12.126		0.916	−4.28	−4.21	20.61	0.02
Co1—C18	1.8409 (3)	0.85 (1)	11.37 (1)	1.841	0.937	−4.24	−4.18	19.78	0.01
		0.861	11.872		0.934	−3.95	−3.78	19.60	0.04
Co1—C19	1.8210 (2)	0.92 (1)	12.65 (1)	1.821	0.930	−4.84	−4.64	22.13	0.04
		0.901	12.160		0.927	−4.18	−4.04	20.37	0.03
Co2—C7	1.9500 (2)	0.65 (1)	8.35 (1)	1.954	1.003	−2.85	−1.19	12.38	1.40
		0.724	6.835		1.000	−3.23	−2.35	12.41	0.38
Co2—C8	1.9863 (2)	0.63 (1)	8.38 (1)	2.023	1.018	−2.65	−0.22	11.24	11.15
		0.665	7.522		1.011	−2.82	−1.37	11.71	1.06
Co2—C20	1.8033 (3)	0.90 (1)	12.22 (1)	1.803	0.924	−4.56	−4.43	21.20	0.03
		0.937	12.020		0.916	−4.19	−4.18	20.39	0.00
Co2—C21	1.8374 (3)	0.86 (1)	11.32 (1)	1.838	0.934	−4.39	−4.24	19.94	0.04
		0.865	11.913		0.932	−3.94	−3.82	19.67	0.03
Co2—C22	1.8165 (2)	0.91 (1)	12.34 (1)	1.817	0.929	−4.78	−4.64	21.76	0.03
		0.910	12.209		0.926	−4.23	−4.06	20.50	0.04
Co3—C9	1.9795 (2)	0.64 (1)	8.45 (1)	2.007	1.014	−2.67	−0.41	11.54	5.45
		0.668	7.415		1.009	−2.86	−1.58	11.85	0.81
Co3—C10	1.9652 (2)	0.66 (1)	8.42 (1)	1.972	1.004	−2.83	−1.19	12.43	1.39
		0.697	6.935		1.006	−3.03	−2.06	12.03	0.48
Co3—C23	1.8027 (3)	0.94 (1)	12.50 (1)	1.803	0.920	−4.79	−4.74	22.03	0.01
		0.937	12.113		0.915	−4.17	−4.15	20.43	0.00
Co3—C24	1.8250 (3)	0.87 (1)	12.25 (1)	1.825	0.933	−4.35	−4.20	20.80	0.04
		0.895	12.097		0.928	−4.15	−3.98	20.23	0.04
Co3—C25	1.8280 (2)	0.89 (1)	12.06 (1)	1.828	0.931	−4.44	21.04	0.02	
		0.887	12.042		0.929	−4.08	−3.95	20.07	0.03
Co4—C9	1.9801 (2)	0.64 (1)	8.38 (1)	1.993	1.012	−2.62	−0.88	11.88	1.98
		0.669	7.393		1.011	−2.87	−1.58	11.84	0.81
Co4—C10	1.9665 (2)	0.64 (1)	8.35 (1)	1.974	1.007	−2.68	−1.06	12.08	1.54
		0.697	6.873		1.007	−3.04	−2.03	11.94	0.496
Co4—C26	1.8045 (3)	0.93 (1)	12.31 (1)	1.805	0.919	−4.70	−4.61	21.62	0.02
		0.935	11.992		0.916	−4.18	−4.14	20.31	0.01
Co4—C27	1.8226 (3)	0.90 (1)	11.87 (1)	1.823	0.929	−4.68	−4.54	21.09	0.03
		0.896	12.120		0.927	−4.15	−3.97	20.24	0.04
Co4—C28	1.8278 (2)	0.91 (1)	12.05 (1)	1.828	0.932	−4.78	−4.59	21.42	0.04
		0.890	12.015		0.930	−4.16	−4.00	20.18	0.04
C7—C8	1.3570 (2)	2.23 (1)	−15.75 (3)	1.360	0.683	−15.1	−14.4	13.8	0.04
		2.192	−19.779		0.673	−13.86	−13.51	7.59	0.03
C8—C9	1.4277 (3)	1.93 (1)	−12.68 (3)	1.428	0.715	−13.4	−13.2	13.9	0.01
		1.882	−16.275		0.716	−12.36	−12.13	8.22	0.02
C9—C10	1.3604 (3)	2.19 (1)	−14.68 (3)	1.363	0.682	−14.7	−13.8	13.7	0.07
		2.193	−19.797		0.686	−14.08	−13.42	7.70	0.05

calculations (Overgaard *et al.*, 2008; Platts *et al.*, 2007), so this method was employed, together with a basis set consisting of 6-31+G(d,p) (Ditchfield *et al.*, 1971) on C, H and O with a Stuttgart–Dresden basis set/effective core potential (Dolg *et al.*, 1987) augmented with a set of f-type polarization functions (Ehlers *et al.*, 1993) on Co, for all theoretical studies of (1). Tests on smaller model systems indicate that the use of effective core potentials on Co does not significantly alter calculated electron-density properties.

Theoretical calculations for (2) employed CASSCF methods, shown previously to be necessary for the accurate description of the singlet biradical nature of the model compound $Co_2(CO)_6C_2H_2$. Atomic coordinates of (2) were extracted from the final multipole model (Overgaard & Platts, 2009), and imported into the *GAUSSIAN*03 suite of programs (Frisch *et al.*, 2004). A basis set consisting of cc-pVDZ (Woon & Dunning, 1993) on all light atoms and 6-31G, augmented with a set of f-type functions, on Co was employed. As in our previous work, several molecular orbitals showed significant deviations from integer populations; those spatially localized to the Co_2C_2 core were identified visually, and employed in CASSCF[6,6] calculations. This choice of active space is based on natural orbital occupation numbers, in which significant deviations from occupations of 2 or 0 are found for six orbitals, and was extensively tested and verified in our previous studies (Platts *et al.*, 2007).

Direct analysis of the resulting theoretical electron density was complemented by the calculation of theoretical structure factors from this CASSCF[6,6] wavefunction. This was achieved by the use of Howard *et al.*'s program *MOON*, specifically designed to work with non-integer molecular orbital (MO) populations (Hibbs *et al.*, 2005). MO coefficients and populations were taken from *GAUSSIAN*03 output data and entered directly into *MOON*, with no attempt to further refine any such parameter, and used to generate theoretical structure factors for subsequent multipole modelling. The number and Miller indices of the generated theoretical structure factors correspond to the measured Bragg intensities. To mimic the experimental conditions, random experimental noise was added to the noise-free theoretical structure factors. This was achieved by creating 1000 different sets of structure factors in which all intensities consist of a sum of the noise-free value and a Gaussian-weighted random number in the range from −1 to 1 multiplied by the standard uncertainty, the latter stemming from the averaging of equivalent measurements [the intensity distribution of reflection (313) is shown in the supplementary material[1] to illustrate the usefulness of the algorithm].

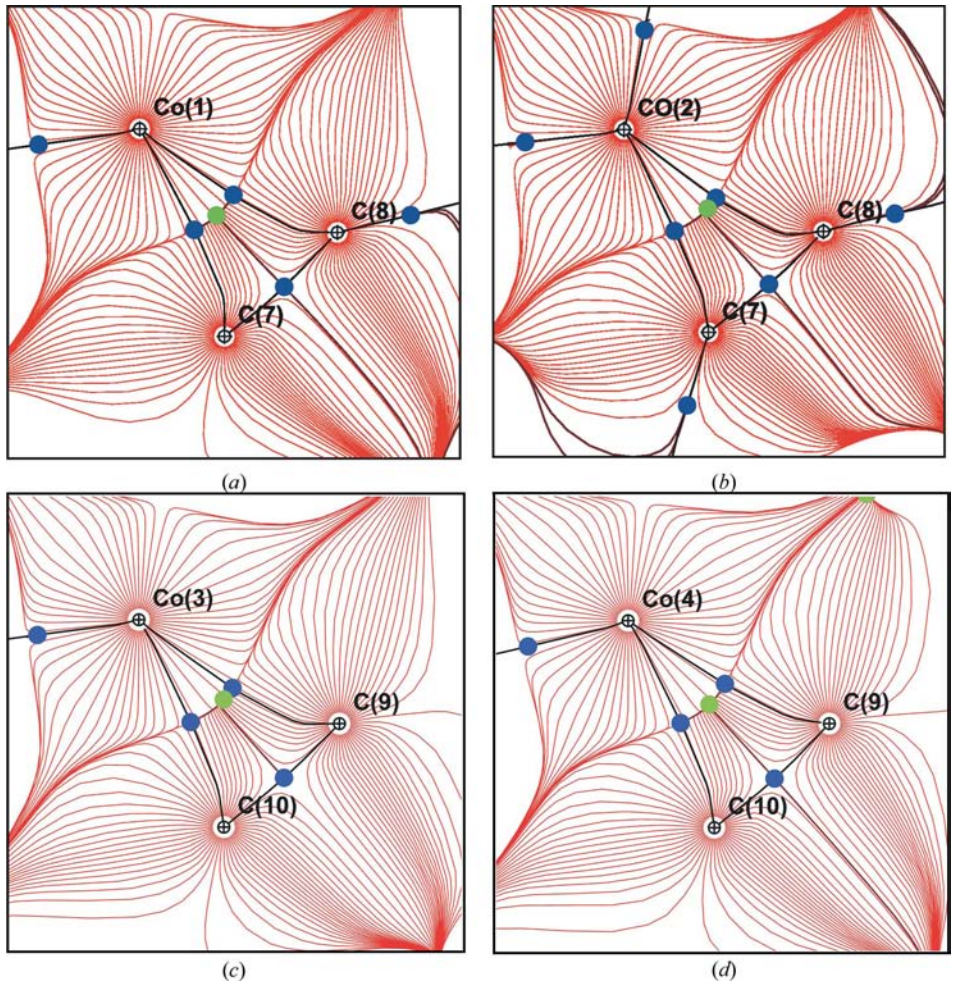

Figure 4
Maps of the density gradients with the molecular graphs superimposed in the four CoC_2 triangles formed by the two triple bonds and the Co atoms from the experimental study of (1). The blue circles indicate b.c.p.s, and the green circles indicate r.c.p.s.

3. Results and discussion

3.1. Electron-density distribution

The complete topological analysis is given in Table 2, together with the bond distances in (1). Before moving the focus to the density in the molecular centres defined by the two Co_2C_2 tetrahedra, a few trends should be noted. There is a clear correlation between the value of $L(r)$ [$L(r) = -\nabla^2\rho_c(\mathbf{r})$] and the bond length such that a shorter bond gives a higher value of $L(r)$. Similarly, the density itself [$\rho_c(\mathbf{r})$] also increases with a shorter bond distance and the exact behaviour resembles closely the trend lines given by Gibbs (Gibbs *et al.*, 2006). In terms of bond distances, the bonds C1—C7 and C10—C11 within the alkyne chain resemble C—C single bonds between two sp^2 C atoms, while the C7—C8 and C9—C10 bonds are much longer than C—C triple bonds and more similar to C—C double bonds. The C8—C9 bond is slightly shorter than a C—C single bond between two sp^2 C atoms. These geometrical considerations are partly supported by the topological analysis of the density. However, the value of the ellipticity (which reflects the asymmetry in the charge distribution in the two directions perpendicular to the interatomic line at the b.c.p.) in what is expected to be C—C double bonds should be significantly increased compared with single and triple bonds, but that is not so. It is very likely that this is due to the fact that the interaction between *p* orbitals centred on the C atoms C7–C10 and the Co atoms leads to an increase in the density on one side of the C—C bond near the C—C b.c.p. and thus diminish the asymmetry, thereby reducing the ellipticity.

[1] Supplementary data for this paper are available from the IUCr electronic archives (Reference: PI5003). Services for accessing these data are described at the back of the journal.

Table 3
Bond distances and bond asymmetries in the two Co_2C_2 centres in (1).

Bond	d(Co—C) (Å)	Length (b.p.) (Å)	δ (Å)	⊥ distance (Å)	Asymmetry
Co1—C7	1.9832 (2)	2.0193	0.0361	0.1208	0.0098
Co1—C8	1.9735 (2)	2.0128	0.0393	0.1258	
Co2—C7	1.9500 (2)	1.9610	0.0110	0.0645	0.0363
Co2—C8	1.9863 (2)	2.0736	0.0873	0.1894	
Co3—C9	1.9795 (2)	2.0397	0.0602	0.1645	0.0143
Co3—C10	1.9652 (2)	1.9792	0.0140	0.0785	
Co4—C9	1.9801 (2)	2.0074	0.0273	0.1126	0.0136
Co4—C10	1.9665 (2)	1.9834	0.0169	0.0847	

3.2. Analysis of the density in the molecular centre

The experimental electron-density distribution (EDD) in the proximity of the molecular centres constituted by the two Co_2C_2 tetrahedra in (1) is illustrated in Figs. 4(*a*)–(*d*), by mapping the gradient of the electron density in the four available CoC_2 planes with the bond paths and the b.c.p.s and r.c.p.s superimposed on the figures. In total, eight Co—C b.c.p.s are anticipated and they are all easily located in (1); however, the exact location of the r.c.p. within the triangles formed by the interatomic vectors in the CoC_2 planes is far from symmetrical in two of the four cases, where it is instead found displaced towards one of the Co—C b.c.p.s. This near-coalescence of an r.c.p. and a b.c.p. is coined a catastrophic situation within the theory of QTAIM and was experimentally observed by Macchi and coworkers a decade ago (Macchi *et al.*, 1998) in a Ni-containing compound. In their refinements they found that hexadecapoles were imperative to retrieve a multipole model without seeing a catastrophe in the topology. In the case of (1) it is possible to instigate such a catastrophe by modification of the multipole model used in the description, for example by allowing a refinement of all parameters. This aspect originates at least partly in the fact that the density along a path between the two Co—C b.c.p.s through the r.c.p. is rather high and very slowly changing. In fact, the difference in the value of the density at the b.c.p. and the r.c.p. is never larger than 0.02 e Å^{-3}, which is of the same magnitude as the uncertainty based on the least-squares procedure.

On closer examination of the geometry and topology in the two Co_2C_2 tetrahedra (Table 2) it appears that the difference (denoted δ) between the length of the Co—C bond path and the length of the Co—C interatomic line – which reveals some information about how bent the bond is – is connected to how distinct the b.c.p. is, and in the event of a complete coalescence the bond path of course disappears. It is obvious that the Co2—C7—C8 triangle is the most asymmetric in terms of Co—C bond distances (last column in Table 3) as it contains both the shortest and the longest Co—C bonds. This is reflected in the δ values, which are the smallest and largest in this triangle. Similarly, the perpendicular distance from the interatomic Co—C line to the b.c.p. increases with increasing δ. In general, it is such that a large asymmetry in the Co—C bond distances induces a clear difference between the characteristics of the two Co—C b.c.p.s and an asymmetric position of the r.c.p. The opposite is also true, as in Co1—C7—C8, which shows a very symmetric position of the r.c.p. However, there are fluctuations in the values and no clear systematic trends can be deduced from this set of values.

For comparison, Fig. 5 shows the theoretical molecular graphs for (1), calculated using DFT, in the same four CoC_2 planes, in which all eight Co—C b.c.p.s are also located. As in the experimental analysis, these plots also show differing degrees of asymmetry in the position of the r.c.p., with the Co2—C7—C8 r.c.p. most notably off-centre. The difference in density between the b.c.p. and the r.c.p. in this plane is just 0.016 e Å^{-3}, in excellent agreement with experimental data. The largest difference between the b.c.p. and the r.c.p. is found in the Co1—C7—C8 plane at 0.040 e Å^{-3}, only slightly larger than the estimated uncertainty in experimental density data and the residual errors shown in Fig. 3. Therefore, it may be that the chances for obtaining an accurate and reliable description of the density comparable to theoretical densities in such an environment may be at the limit of what is currently achievable by modelling with intrinsically noisy experimental structure factors.

To probe this in more detail we have calculated theoretical structure factors and fitted a multipole model to these, thus allowing us to examine separately the effects of noisy data and the potential limitations of the multipole model. However, as mentioned above the complexity and size of (1) is of such a scale that the calculation of theoretical structure factors is impractical and a simpler molecule is required for this procedure. Therefore, we turned to the previously studied cobalt dimer complex, $[Co(CO)_3]_2PhC{\equiv}CPhNO_2$ (2), for which we have previously measured high-resolution X-ray diffraction data and studied the resulting charge distribution (Overgaard & Platts, 2009).

3.3. Noise-free theoretical structure factors

It is a problem of some significance that inherent limitations apply to the widely used multipole model. For example, it has

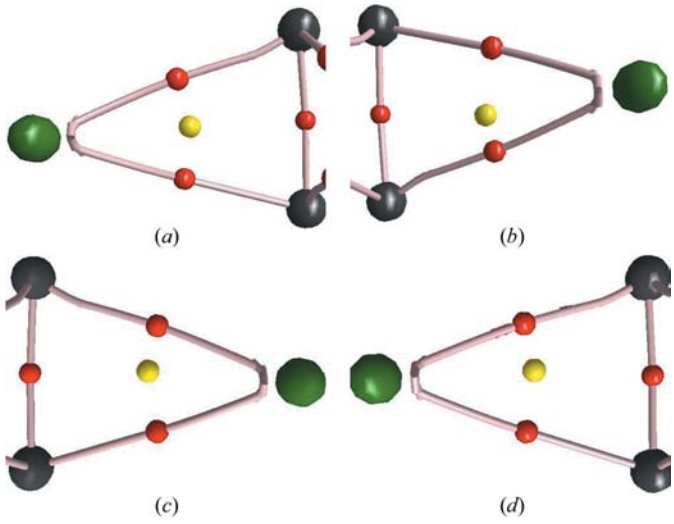

Figure 5
Theoretical molecular graphs for (1). Red dots indicate a b.c.p. and yellow dots indicate an r.c.p. The atoms shown are the same as those in Fig. 4.

been shown using theoretical structure factors that the single-zeta Slater-type radial functions used in the modelling are too rigid or inflexible to satisfactorily describe the detailed density distribution and that more advanced treatments such as several independent sets of radial density functions on each atom can improve the fit significantly (Figgis *et al.*, 1993; Iversen *et al.*, 1997; Volkov & Coppens, 2001; Koritsanszky & Volkov, 2004; Dittrich *et al.*, 2007). Initially we have therefore used the calculated structure factors as the input for a least-squares refinement of a multipole model very similar to the experimental description of (1) and studied the effect this has on the electron density, with particular emphasis on the sensitive CoC_2 planes. The density derived directly from the CASSCF calculations (denoted 'T' in Fig. 6*a*) gives clear maxima for all Co—C b.c.p. positions. These clear trends are dampened somewhat by the multipole modelling (denoted 'TM' in Fig. 6*b*) of the generated structure factors, to the extent that one of the b.c.p.s (Co1—C12) has a much lower curvature of the density along the r.c.p.–b.c.p. direction and is significantly closer to the r.c.p. (0.112 Å compared with 0.259 Å from the primary density). However, the overall tendencies of the density profiles are conserved such that within one CoC_2 triangle one of the Co—C b.c.p.s is more significant than the other, and each C atom is involved in one clear b.c.p. and one 'vague' b.c.p. It is also evident that distances between b.c.p.s and r.c.p.s are largest for the most significant b.c.p.s, while the less distinct b.c.p.s are closer to the r.c.p. This is in complete accordance with the observations given in the previous section on the analysis of (1).

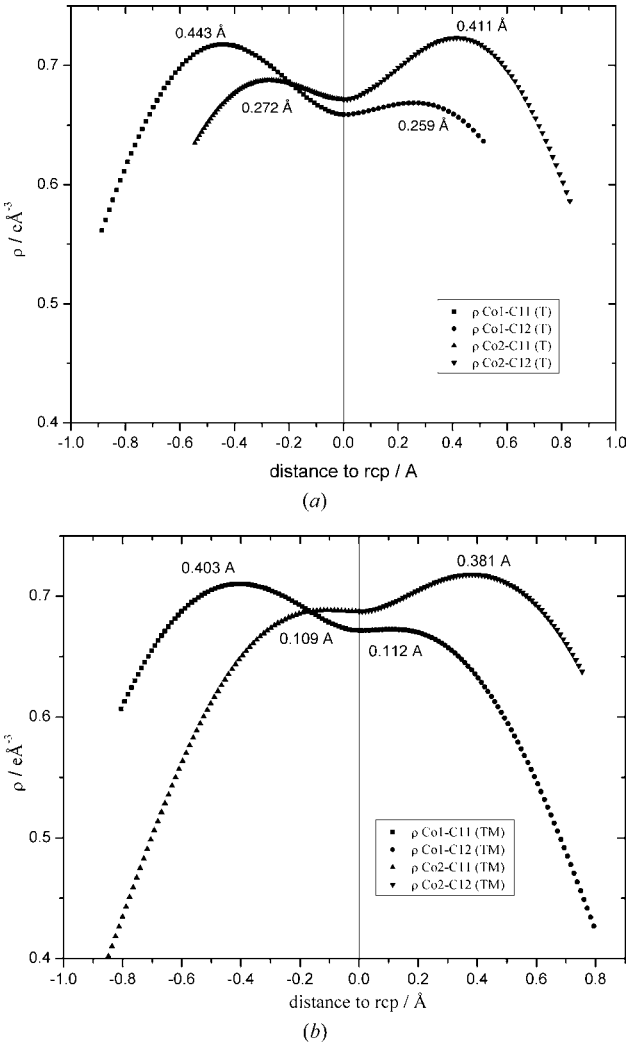

Figure 6
Electron density along the b.c.p.–r.c.p.–b.c.p. path in the CoC_2 planes of (2). (*a*) Directly from theory; (*b*) multipole modelling of theoretical structure factors. The bond distances in (2) for the four Co—C bonds in the order given in the figure captions are (Å): 1.9490 (5), 1.9858 (5), 1.9757 (5) and 1.9502 (5). The distances from the r.c.p. to the respective b.c.p.s are denoted on the figures.

3.4. 'Noisy' theoretical structure factors

To probe the effects of measurement noise on the multipole modelled density, random perturbations were added to the calculated structure factors, employing a Gaussian distribution of pseudo-random numbers based on the experimental s.u.s, the latter taken directly as the statistical errors from merging of equivalent reflections. This procedure was repeated 1000 times, to ensure any effects observed are not simply an artefact of the random number generator employed. The average density over these 1000 noisy refinements was calculated in the plane spanned by Co2 and the C11—C12 bond, and is depicted in Fig. 7(*a*), which shows two separable maxima and a minimum in between. Thus, it appears that the average density from the noisy data is rather similar to the density from the noise-free data, at least near the atomic boundaries. However, there are significant differences between the average density and the noise-free model close to the atomic positions, while in the interatomic regions the differences are almost vanishing (Fig. 7*b*). The r.m.s. value (Fig. 7*c*) in the regions around the b.c.p.s are of the order 0.01 e $Å^{-3}$, which is comparable to the uncertainties estimated from the least-squares procedure. Qualitatively, this is revealed by Fig. 7(*d*), which is highly similar to Fig. 7(*a*).

The influence from the addition of noise to the theoretical structure factors is more evident from a topological analysis of individual total densities. The proximity of two b.c.p.s and an r.c.p., along with the rather flat electron density between them, makes the topology very sensitive to model changes. Fig. 8 demonstrates that only in 41% of the models (purple partition) are all four b.c.p.s located as they are in the model based on the noise-free data, while in 45% of the cases (light and dark blue) one of either Co1—C12 or Co2—C11 is missing. It is not unexpected that the recovery of these two particular b.c.p.s is difficult as the CoC_2 triangles hold one long bond and one short Co—C bond, and the two mentioned bonds represent the longer one. In a significant fraction of cases (green, 14%) both of these b.c.p.s are absent. In less than 1% of cases, the addition of simulated noise prevents the multipole model from locating one of the more clearly defined b.c.p.s, while it does not happen that all four b.c.p.s are missing in the same model density. Thus, the presence of random noise in the raw data has a substantial effect on the topology of the electron density in this highly sensitive region.

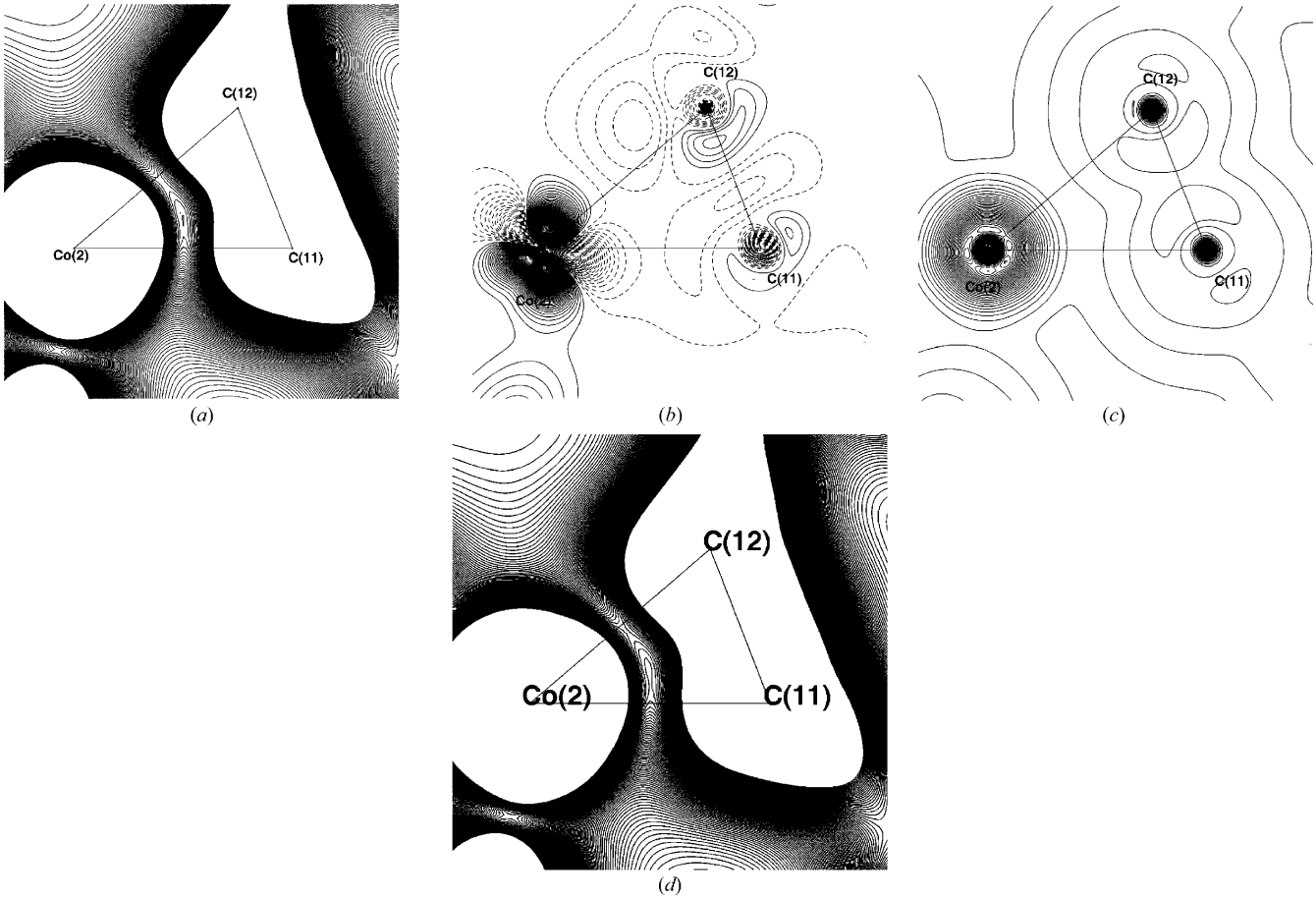

Figure 7
Density profiles in the plane of the Co2—C11—C12 triangle resulting from 2σ modifications of the theoretical structure factors. The first row shows the average density, the difference density (*i.e.* the average subtracted the unmodified density) and the root-mean-square deviation from the average. The second row shows the total density from the multipole model of the noise-free data. The contour interval is chosen as small as 0.01 e Å^{-3} to highlight bonding features; positive contours are shown with solid lines and negative (where appropriate) are given by dashed lines.

It is of interest to examine further the contributions from the different multipole parameters, both considering all 1000 models as a complete set and also within each group shown in Fig. 8. The statistical analysis of the whole set unsurprisingly reveals average values of the multipole parameters close to the refined values from the noise-free data set (for Co1 the average root-mean-square deviation between the values of the refined and the 1000 set average for all multipole parameters including P_v is as small as 0.00061) with standard deviations corresponding well to the least-squares derived s.u.s.

We have also examined the distribution of multipole parameters within each of the six subsets outlined in Fig. 8 in order to locate systematic differences that could be responsible for the different topologies. However, the average values from each subset for the different multipole parameters cluster around very similar values and the standard deviations of the average values are much larger than the spread observed (an illustration for both Co1 and C11 is shown in the supplementary material). It is therefore not possible, based on this statistical analysis, to point out which parameters, if any, are mainly responsible for the change of topology. This is also perhaps not surprising given the fact that the necessary changes in the total density to accommodate a change in topology are extremely small.

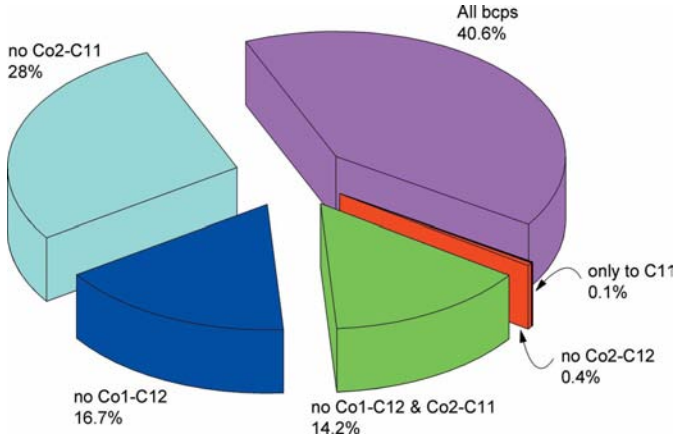

Figure 8
Distribution of b.c.p.s obtained from the refinement of 'noisy' theoretical structure factors.

4. Conclusions

We have used multipole modelling of high-resolution X-ray diffraction data, coupled with theoretical calculations, to study the electron density in two alkyne-bridged dicobalt species, with particular reference to the highly sensitive nature of the topology of the density within the Co_2C_2 core. Data for (1) were of sufficient quality to obtain a reliable multipole model of the electron density, from which all eight expected b.c.p.s could be located. However, differences in the detailed positions of b.c.p.s and r.c.p.s were observed across the four CoC_2 planes, with significant asymmetry and resulting proximity of b.c.p. and r.c.p. in two such planes. This topological situation is close to a 'catastrophe point', where critical points merge, with further evidence for the sensitive nature of the density in such regions coming from a difference in electron density of just 0.02 e $Å^{-3}$. Direct calculation of electron density for (1) using density-functional theory supports these conclusions, in that all eight b.c.p.s are located in this manner, but with noticeable asymmetry and small differences in density between b.c.p.s and r.c.p.s.

Unfortunately, crystal quality meant that diffraction data for complex (2) was not of a sufficient standard to obtain a reliable multipole model. However, this complex was suitable for calculation of theoretical structure factors from *ab initio* data, which enabled us to examine any limitations of the multipole model in this case, and also to simulate the effects of random measurement noise in derived density properties. Structure factors were calculated from a CASSCF[6,6] wavefunction that properly represents the singlet biradical character of (2), incorporating non-integer MO occupations. A multipole model of this theoretical data reproduces the topology of the direct, *ab initio* density, but also appears to 'flatten' the density in the CoC_2 plane somewhat. The addition of random noise prior to multipole modelling has a significant effect on the topology observed, with almost two-thirds of models derived missing at least one b.c.p. compared with noise-free models.

We thank the referees for useful comments.

References

Allen, F. H., Kennard, O., Watson, D. G., Brammer, L., Orpen, A. G. & Taylor, R. J. (1987). *J. Chem. Soc. Perkin Trans. II*, pp. 1–19.

Bader, R. F. W. (1990). *Atoms in Molecules: A Quantum Theory*. Oxford: Clarendon Press.

Bader, R. F. W. & Gatti, C. (1998). *Chem. Phys. Lett.* **287**, 233–238.

Becke, A. D. (1988). *Phys. Rev. A*, **38**, 3098.

Bianchi, R., Gervasio, G. & Marabello, D. (1998). *Chem. Commun.* pp. 1535–1536.

Bianchi, R., Gervasio, G. & Marabello, D. (2001). *Acta Cryst.* B**57**, 638–645.

Blessing, R. H. (1989). *Crystallogr. Rev.* **1**, 3–58.

Blessing, R. H. (1997). *J. Appl. Cryst.* **30**, 421–426.

Bruker (2007*a*). *APEX*2. Bruker AXS Inc., Madison, Wisconsin, USA.

Bruker (2007*b*). *SAINT*+, Version 7.34A. Bruker AXS Inc., Madison, Wisconsin, USA.

Cremer, D. & Kraka, E. (1984*a*). *Angew. Chem. Int. Ed. Engl.* **23**, 627.

Cremer, D. & Kraka, E. (1984*b*). *Croat. Chem. Acta*, **57**, 1259.

Ditchfield, R., Hehre, W. J. & Pople, J. A. (1971). *J. Chem. Phys.* **54**, 724.

Dittrich, B., Koritsanszky, T., Volkov, A., Mebs, S. & Luger, P. (2007). *Angew. Chem. Int. Ed.* **46**, 2935–2938.

Dolg, M., Wedig, U., Stoll, H. & Preuss, H. (1987). *J. Chem. Phys.* **86**, 866.

Ehlers, A. W., Böhme, M., Dapprich, S., Gobbi, A., Hijllwarth, A., Jonas, V., Kiihler, K. F., Stegmann, R., Veldkamp, A. & Frenking, G. (1993). *Chem. Phys. Lett.* **208**, 111–114.

Farrugia, L. J. & Evans, C. (2005). *J. Phys. Chem. A*, **109**, 8834–8848.

Farrugia, L. J., Mallinson, P. R. & Stewart, B. (2003). *Acta Cryst.* B**59**, 234–247.

Figgis, B. N., Iversen, B. B., Larson, F. K. & Reynolds, P. A. (1993). *Acta Cryst.* B**49**, 794–806.

Finger, M. & Reinhold, J. (2003). *Inorg. Chem.* **42**, 8128–8130.

Flierler, U., Burzler, M., Leusser, D., Henn, J., Ott, H., Braunschweig, H. & Stalke, D. (2008). *Angew. Chem. Int. Ed.* **47**, 4321–4325.

Frisch, M. J. *et al.* (2004). *GAUSSIAN*03, Revision C.02. Gaussian, Inc., Wallingford, CT.

Gatti, C. & Lasi, D. (2007). *Faraday Discuss.* **135**, 55–78.

Gibbs, G. V., Spackman, M. A., Jayatilaka, D., Rosso, K. M. & Cox, D. F. (2006). *J. Phys. Chem. A*, **110**, 12259–12266.

Greenfield, H., Sternberg, H. W., Friedel, R. A., Wotiz, J. H., Markby, R. & Irving, M. (1956). *J. Am. Chem. Soc.* **78**, 120–124.

Hansen, N. K. & Coppens, P. (1978). *Acta Cryst.* A**34**, 909–921.

Hibbs, D. E., Howard, S. T., Huke, J. P. & Waller, M. P. (2005). *Phys. Chem. Chem. Phys.* **7**, 1772–1778.

Hirshfeld, F. L. (1976). *Acta Cryst.* A**32**, 239–244.

Iversen, B. B., Larsen, F. K., Figgis, B. N. & Reynolds, P. A. (1997). *J. Chem. Soc. Dalton Trans.* pp. 2239–2347.

Koritsanszky, T. & Volkov, A. (2004). *Chem. Phys. Lett.* **385**, 431–434.

Lee, C., Yang, W. & Parr, R. G. (1988). *Phys. Rev. B*, **37**, 785.

Macchi, P. (2005). *J. Am. Chem. Soc.* **127**, 17593–17594.

Macchi, P., Garlaschelli, L., Martinengo, S. & Sironi, A. (1999). *J. Am. Chem. Soc.* **121**, 10428–10429.

Macchi, P., Proserpio, D. M. & Sironi, A. (1998). *J. Am. Chem. Soc.* **120**, 1447–1455.

Madsen, A. Ø. (2006). *J. Appl. Cryst.* **39**, 757–758.

Meindl, K. & Henn, J. (2008). *Acta Cryst.* A**64**, 404–418.

Munshi, P., Madsen, A. Ø., Spackman, M. A., Larsen, S. & Destro, R. (2008). *Acta Cryst.* A**64**, 465–475.

Overgaard, J., Clausen, H. F., Platts, J. A. & Iversen, B. B. (2008). *J. Am. Chem. Soc.* **130**, 3834–3843.

Overgaard, J. & Platts, J. A. (2009). Unpublished results.

Platts, J. A., Evans, G. J. S., Coogan, M. P. & Overgaard, J. (2007). *Inorg. Chem.* **46**, 6291–6298.

Schomaker, V. & Trueblood, K. N. (1968). *Acta Cryst.* B**24**, 63–76.

Sheldrick, G. M. (2008). *Acta Cryst.* A**64**, 112–122.

Volkov, A. & Coppens, P. (2001). *Acta Cryst.* A**57**, 395–405.

Volkov, A., Macchi, P., Farrugia, L. J., Gatti, C., Mallinson, P. R., Richter, T. & Koritsánszky, T. S. (2006). *XD*2006. University of New York at Buffalo, NY, USA.

Woon, D. E. & Dunning Jr, T. H. (1993). *J. Chem. Phys.* **98**, 1358.